Behaviour of saturated railway track foundation materials during undrained cyclic loading

Anna Mamou1 anna_mamou@yahoo.com
Jeffrey A. Priest2 japriest@ucalgary.ca
Christopher R. I. Clayton1 cric@soton.ac.uk
William Powrie1* wp@soton.ac.uk

***Corresponding Author's Name: William Powrie**

1University of Southampton School of Civil and Environmental Engineering
Highfield , Southampton SO17 1BJ U.K.

2University of Calgary - Civil Engineering, 2500 University Drive N.W.,
Calgary, Alberta T2N 1N4 Canada

Abstract: This paper presents the results of a series of hollow cylinder tests carried out to investigate the undrained behaviour of saturated railway track foundation materials during cyclic loading involving principal stress rotation. Four sand-clay mixes representative of real railway track foundation materials were investigated. It was found that moderate additions of clay (up to ~14% by weight) increased the cyclic shear stress threshold at which significant excess pore pressures started to accumulate. After the cyclic shear stress threshold had been exceeded, the rate of pore pressure increase with the logarithm of the axial strain was greatest for the material having a clay content of 11%. Excess pore pressure generation reduced with increasing intergranular and global void ratio, with the global void ratio being perhaps the more useful indicator because of the reduced amount of scatter and higher correlation of the idealized relationship.

Keywords: Hollow cylinder apparatus, cyclic tests, principal stress rotation, excess pore pressure, sand, silt, clay, global void ratio, intergranular void ratio

All data supporting this study are openly available from the University of Southampton repository at http://doi.org/10.5258/SOTON/D0256"

BACKGROUND

Historically, most railway track foundations were constructed using empirical design methods based on results of simple static soils tests ignoring the effects of repeated wheel loads. This may have contributed to premature loss of serviceability of railway track through geometry deterioration, and associated high maintenance costs.

Improved design guidelines, based on results from cyclic triaxial tests in which the wheel load is modelled as a cyclic axial stress (e.g. AREA 1996), still do not adequately represent the true stress regime imposed by trains on a soil element in the railway track foundation (Brown et al. 1975; O'Reilly et al. 1991; Shahu et al. 1999). As trains approach or recede, and accelerate or brake over a section of track, the soil below experiences changes in vertical and horizontal normal and shear stresses, equivalent to a rotation of the principal stress directions (Brown 1996).

Cyclic changes in the principal stress directions have been shown to affect the development of plastic strains (Chan and Brown 1994; Cai et al. 2015; Guo et al. 2017). The effects of principal stress rotation (PSR) on the rate of plastic strain accumulation reduce as the clay content increases (Gräbe and Clayton 2009). PSR may also reduce the saturated resilient modulus of a specimen by approximately 20–26%, depending on the overconsolidation ratio (OCR), the clay content, and the consolidation regime followed in preparing the specimen (Gräbe and Clayton 2014).

The effect of fines on the susceptibility of a sand to generate pore pressures and plastic strains has previously been investigated in strain controlled cyclic triaxial tests (e.g. Vucetic and Dobry1988; Erten and Maher 1995), and generally been observed to have little or no effect below a certain cyclic strain threshold. Significant excess pore pressures and strains develop as the cyclic strain threshold is exceeded, with the fines content controlling the amount of excess pore pressures generated. However, the direct application of these observations to railway track foundation design is uncertain, because

i. stresses are generally more easily quantified than strains;

ii. it is difficult to relate the cyclic strain threshold to a corresponding cyclic stress because of the varying stiffnesses of the different materials; and

iii. observations on the effect of fines on the pore pressure generation of the sand made in the context of stress controlled cyclic triaxial tests which generally involve testing at high cyclic stress ratios may not be representative of railway track foundations, where the stress path involves cyclic stress amplitudes considerably smaller than the initial mean effective stress (Amini and Qi 2000; Polito and Martin 2001; Bray and Sancio 2006), as well as principal stress rotation.

Numerical modelling and field tests have indicated that although vertical stresses during train passage attenuate with depth, horizontal stress changes become more pronounced up to a certain depth below the sleeper base before then reducing at greater depths (Powrie et al. 2007; Priest et al. 2010). In addition to the stress changes due to vertical loads, stress changes resulting to the along-track forces applied during train acceleration and/or braking may also be significant. Powrie et al. (2007) noted that a maximum horizontal force of 25% of the wheel load applied during acceleration and/or braking increased the horizontal (along the track) shear stresses at the top of the foundation by 6% and at the bottom by 9% of the values calculated with a purely vertical moving load.

The rotations in principal stress direction caused by these changes in horizontal and shear stress may have a significant effect on the stability of railway track foundations, but have not been widely investigated (Gräbe and Clayton 2009). The current paper aims to address this knowledge gap by investigating the influence of cyclic shear stress changes on the axial strain, pore pressure, resilient stiffness and susceptibility to failure of a range of soils used in railway track foundations. It draws on laboratory test data from materials having clay contents of 7-14% (Materials A to C) previously reported by Mamou et al. (2017), as well as data on a material having a clay content of 24% (Material D), and discusses the generation of excess pore water pressures in undrained conditions in more detail.

EXPERIMENTAL METHOD

Apparatus

Laboratory tests to investigate the behaviour of railway foundation material under different loading conditions were carried out using a hollow cylinder apparatus (HCA). In the HCA, a hollow cylindrical specimen is subjected to an axial load, torque about a central vertical axis and internal and external radial pressures. The axial load gives rise to an axial stress σ_z, and the torque induces shear stresses $\tau_{z\theta}$ on the horizontal planes and complementary shear stresses $\tau_{\theta z}$ on the vertical radial planes. The combination of axial stress and torque can be used to control the magnitude and orientations of the principal stresses.

In the HCA, stress-strain non-uniformities can arise across the specimen owing to the application of the torque and different internal and external cell pressures. The torque can lead to variations in $\tau_{z\theta}$ across the specimen wall, while a difference between the inner and outer cell pressures can change the curvature resulting in variations in radial and circumferential stresses. To minimise these stress-strain non-uniformities and their effects, the inner and outer chamber (cell) pressures were kept equal and the data were interpreted using the Hight et al. (1983) framework of average stresses and strains. The average stresses were corrected to take into account the effect of membrane restraint using the approach given by Tatsuoka et al. (1986; their Equations 8-10). Correction for membrane penetration effects was unnecessary, as the specimens were fine grained and well graded, prepared at relatively high dry densities and tested at low effective stresses.

The resilient modulus of a soil, E_r, is the stiffness calculated from the recoverable (i.e. resilient) strains under repeated loading / unloading. In the HCA, the resilient modulus is equivalent to the resilient Young's modulus given by:

$$E_r = q/\varepsilon_a \tag{1}$$

where q is the cyclic deviator stress and ε_a is the recoverable axial cyclic strain.

To obtain realistic values for E_r, axial strains were measured locally on the specimen to avoid errors associated with the misalignment of specimen ends, bedding, and apparatus compliance (Jardine et al. 1984; Clayton and Khatrush 1986; Cuccovillo and Coop 1997). The change in the outer diameter of the specimen was measured using an LVDT attached to a radial caliper. The current inner radius r_i (Eq. 2, for use in the Hight et al (1983) equations, was calculated from the change in inner volume, ΔV_i, assuming the specimen retained a circular cross section during deformation.

$$r_i = r_{io}\sqrt{\frac{1+(\Delta V_i/V_i)}{1+(\Delta H/H)}} \tag{2}$$

where V_i and H are the initial and ΔV_i and ΔH are the changes in the inner volume and specimen height respectively.

Global angular displacements were measured by the torsional actuator shaft encoder. The axial force F and the torque T were measured using a combined load and torque cell located at the top of the specimen. The inner and outer cell pressures and the applied back pressure were controlled by GDS pressure/volume controllers. Pore water pressures were measured independently at the top and bottom of the specimen using Druck PDCR810 pressure transducers, which were calibrated against a 580 series hydraulic dead-weight tester manufactured by DH Budenberg Ltd. to have an accuracy better than 0.34kPa (Mamou 2013). During the undrained cyclic loading tests the top and bottom excess pore pressure readings were generally similar, except for the 24% clay which showed a maximum deviation of around 3kPa. In this paper, the excess pore pressure is taken as the average of the top and bottom excess pore pressure readings.

Materials

Four sand/clay mixes made up of varying proportions of Leighton Buzzard sand fractions B (LBSFB), C (LBSFC) and D (LBSFD); Hymod Prima clay (HPC); and Oakamoor HPF5 silica flour silt were investigated. The sand-clay mixes were selected to represent typical gradations of railway track foundation materials used on the South African Coal Line (Gräbe and Clayton 2009). The compositions of the various mixes as a percentage of the total dry specimen weight, and the specific gravities of the constituent aggregates are given in Table 1.

Specimens were prepared by compaction to a target dry density of ~2.15Mg/m^3, varying the compaction energy and initial water content with the clay content as appropriate. For example, the 11% clay mix was compacted at 8.31% water content in 6 layers with 25 blows per layer, while the 24% clay content mix was compacted at 8.61% water content in 12 layers with 50 blows per layer.

The effect of increasing the clay content is apparent in both the global and intergranular void ratios. The global void ratio e is defined as the ratio of the volume of voids to the volume of solids in a soil element, and considers a void as a space occupied neither by sand nor by fine particles. The global void ratio e_{glob} was calculated as

$$e_{glob} = \frac{V_{voids}}{\frac{\mathrm{M}_{sand}}{G_{s\,sand}\rho_{water}} + \frac{\mathrm{M}_{silt}}{G_{s\,silt}\rho_{water}} + \frac{\mathrm{M}_{clay}}{G_{s\,clay}\rho_{water}}} \tag{3}$$

where M_{sand}, M_{silt} *and* M_{clay} are the mass, and $G_{s\,sand}$, $G_{s\,silt}$ *and* $G_{s\,clay}$ are the grain specific gravities of the sand, silt and clay respectively, ρ_{water} is the density of the water, and V_{voids} is calculated as V_{total} - V_{solids}.

The inter-granular void ratio $e_{intergr}$ for a mixed soil (Mitchell 1976) reflects the notion that up to a certain fines content, the fines occupy voids between the sand grains and do not actively participate in force transmission, hence should be treated as voids. The intergranular void ratio $e_{intergr}$ was calculated as

$$e_{intergr} = \frac{V_{voids} + \frac{M_{silt}}{G_{s\,silt}\rho_{water}} + \frac{M_{clay}}{G_{s\,clay}\rho_{water}}}{\frac{M_{sand}}{G_{s\,sand}\rho_{water}}} \quad (4)$$

where the symbols have the same meanings as in Equation (3). Table 2 summarizes the dry densities, water content and the global and intergranular void ratios for the four clay contents investigated.

Test procedure

Over the life of a railway track foundation, the water content is likely to vary leading to the development of suctions in the soil. Both the suction and the soil stiffness increase as the water content reduces (Otter et al. 2015). Testing the soil in saturated conditions, with minimal or zero suctions, is likely to result in an underestimation of the soil stiffness in the field. However, saturated conditions are likely to be experienced over at least part of the year in temperate wet climates, and were therefore chosen as a convenient and repeatable reference for this research.

The saturation process involved flushing the formed specimens with CO_2 and de-aired water followed by simultaneous increases in cell pressure (inner and outer) and pore pressure, to maintain a constant effective stress. Saturation was confirmed by a final B-value in excess of 0.97 (Black and Lee 1973). Specimens were then consolidated to an isotropic effective stress of 33kPa to represent typical in-situ effective stresses below an unloaded railway track (Gräbe 2001; Powrie et al. 2007; Indraratna et al. 2015).

Thereafter, each specimen was subjected to cycles of axial stress of 0 to 30kPa, together with cycles of shear stress, $\pm\Delta\tau_{\theta z}$, of gradually increasing magnitude. The magnitude of the peak cyclic shear stress, $|\Delta\tau_{\theta z}|$= 8.5kPa, was initially chosen to represent the peak shear stress on a soil element 1 m below the sleeper soffit of a railway track (Powrie et al. 2007). Thereafter, the magnitude of the peak cyclic shear stress was increased in increments until failure occurred. As a point of reference, the cyclic shear stress for a soil element at a depth of 0.3 m below the sleeper base (corresponding to the bottom of a standard 0.3 m thick layer of ballast) was $|\Delta\tau_{\theta z}|$~ 24 kPa (Powrie et al. 2007).

In all tests, a sinusoidal axial stress pulse was cycled 90 degrees out of phase with a sinusoidal shear stress pulse $\pm\Delta\tau_{\theta z}$ as indicated in Fig. 2. The loading frequency used in the tests was 0.0083Hz or approximately 30 cycles per hour, at which a consistent response of the test control software could be achieved. The in situ cyclic loading frequency associated with train passage will be much higher; however, the quasi-static soil response depends on the loading frequency in relation to the soil permeability and the drainage path length, as discussed by Mamou et al. (2017). The essential point is that the rate of loading combined with the drainage conditions imposed in the current tests gave a substantially uniform pore pressure distribution within the specimen, representative of undrained conditions in the field.

The number of loading cycles imposed in each test stage was generally about 700. Although orders of magnitude less than in the field, this was sufficient to bring the specimen to either a stable resilient state or to failure in each case.

At the end of every undrained test stage and before the start of the next, specimens were allowed to drain so as to dissipate any accumulated excess pore pressure; with the resting period varying depending on the clay content.

The stress cycles applied in all of the PSR test stages reported in this paper are summarised in Table 3. The first letter of each test series identifies the drainage condition (U for undrained, F for free to drain), the second letter denotes the type of material (A-D) and the number that follows gives the magnitude of the cyclic shear stress imposed during that stage. Before an undrained test stage, the specimen was subjected to a free-to-drain preloading stage with cyclic PSR (denoted P), to bring specimens to a consistent initial state.

RESULTS AND DISCUSSION

In this section, the stiffness and pore pressure generation data obtained from the hollow cylinder tests are reviewed and compared. Intuitively, it might be expected that adding clay fines to a sand would increase pore pressure generation, decrease the resilient stiffness and increase permanent strains. While this may be so at higher clay contents, for the range of clay content investigated, it will be seen that our data are counterintuitive in this respect. With small additions of clay, cyclic permanent axial strain and excess pore pressures are reduced, as is the rate of post-threshold stiffness degradation. On the basis of this, it may be postulated that with moderate additions of clay (from 7% up to 14% clay by dry weight), the soil structure consists primarily of frame-supporting sand grains, with clay infill acting to improve the point contacts and to some extent as avoid filler, thereby increasing the stability of the overall mix. At higher clay contents, there is enough clay to separate the sand grains, resulting in little grain-to-grain contact of the sand-sized material and the sand grains acting as isolated stiff inclusions within an essentially clay matrix.

Axial strain and excess pore pressures

The accumulation of permanent axial strain with increasing clay content and increasing magnitude of cyclic shear stress is presented in Figure 3. The start of each of the different test stages (i.e., an increase in

magnitude of cyclic shear stress) is indicated by the letters (a) to (c). In all cases, a cyclic shear stress threshold may be identified, above which the residual axial strain and pore water pressure at the end of each cycle begin to accumulate. Each threshold has an associated axial strain.

The results suggest that the cyclic shear stress threshold for the development of significant permanent strains is affected by moderate additions of clay, up to about 14% (by dry weight) (Mamou et al., 2017). Increasing the clay content from 7% to 14% resulted in an increase in the cyclic shear stress threshold of the materials. However, no further increase in the cyclic shear stress threshold occurred when the clay content was increased to 24%.

The influence of clay on the generation of excess pore pressure with the number of cycles of increasing cyclic shear stress is illustrated in Figure 4. Increasing the clay content reduced the tendency for excess pore pressure generation at a given cyclic shear stress; for Material A excess pore pressure started to accumulate at an applied shear stress of 8.5 kPa (stage a), for material B at 11.5 kPa (stage b), and for materials C and D at 14.5 kPa. The increase in the cyclic shear stress at which significant excess pore pressures started to accumulate was most pronounced for increases in clay content over the range 7% to 14%. The subsequent increase in clay content to 24% had little or no tangible effect on either the cyclic shear stress threshold or the corresponding axial strain.

The relationships between axial stain and excess pore pressure ratio R (defined as the excess pore water pressure divided by the effective stress at the start of the test) for the four materials investigated are shown in Figure 5. Indicative data points for each clay content are presented along with the least squares regression lines calculated for all data using Sigma Plot (Statistical Software Inc. 1994). Increasing the clay content from 7% to 14% increased the axial strain at which significant residual excess pore water pressure started to be generated. The subsequent rate of pore pressure ratio increase with the logarithm of the axial strain, $dR/d(\log_{10}\varepsilon_a)$, increased sharply as the clay content was increased from 7% to 11%, but then gradually reduced with the further addition of clay up to 24%. The post-threshold rate of pore

pressure ratio increase with the logarithm of the axial strain, dR/d($\log_{10}\varepsilon_a$), was similar for clay contents of 7% and 24%, although the cyclic shear stress threshold was considerably higher in the latter case.

To investigate the effect of increasing the clay content on the tendency for excess pore pressure generation, the data were analysed in the context of both the global and intergranular void ratios. Use of the intergranular void ratio implies that the clay may be treated as void space as far as the sand matrix is concerned, while the global void ratio treats the clay particles as contributing to the volume of solids.

Figure 6 shows the variation in excess pore pressure ratio with (a) intergranular and (b) global void ratio for axial strain excursions of 0.25%, 0.75% and 1.00%, for all four materials. The data suggest that excess pore pressure generation reduces with intergranular void ratio at a similar rate for all materials at a given strain, but increases with increasing strain. The scatter in the data at 0.25% axial strain is associated with the significant excess pore pressures developed at this stage for Material A (7% clay), at which Materials B-D generated insignificant excess pore pressures. Excess pore pressure generation also decreased with global void ratio, again with no obvious difference between the different materials. There is more variation between the slopes of the lines at different strains in this case, but the reduced amount of scatter and higher correlation coefficients (R^2) suggest that the relationship between excess pore pressure and global void ratio is more useful than that between excess pore pressure and intergranular void ratio. It is possible that the intergranular void ratio is only relevant at clay contents low enough not to interfere with the packing of the coarser fraction(s).

Resilient modulus

The changes in resilient modulus with the number of cycles of increasing cyclic shear stress for Materials B, C and D (11%, 14% and 24% clay) are shown in Figure 7[1]. Material D (24% clay) exhibited a generally similar pattern in terms of changes in the resilient modulus as previously established for

[1]Material A failed at the lowest cyclic shear stress applied ($\Delta\tau_{\theta z}$ = 8.5kPa) and therefore showed a continuous decrease in resilient modulus from the outset.

Materials B and C (Mamou et al., 2017). Below the cyclic stress threshold increasing magnitudes of cyclic shear stress had little or no effect on the resilient modulus, which for a given material remained broadly similar (85, 105 and 100 MPa for Materials B, C and D respectively) with less than 20% variation between the different material types.

Only after the cyclic shear stress threshold was exceeded did significant stiffness degradation occur. Increasing the clay content to 24%, reduced the rate of post-threshold stiffness degradation with increasing numbers of cycles dE_r/dN to ~0.03MPa/cycle, from ~0.10 MPa/cycle for clay contents of 11% and 14% (Materials B and C) respectively.

Stress paths relative to the critical state line

Figure 8 shows stress paths followed by specimens A-D in terms of deviator stress q, defined in the conventional way as

$$q=\frac{1}{\sqrt{2}}\sqrt{(\sigma'_1-\sigma'_2)^2+(\sigma'_1-\sigma'_3)^2+(\sigma'_2-\sigma'_3)^2} \quad (4)$$

divided by the critical state parameter M as determined for each material by Gräbe and Clayton (2009), (i.e. q/M), plotted against the mean effective stress p' for the undrained test stages of Materials A, B, C and D that caused failure (test stages UA8.5, UB11.5, UC14.5 and UD14.5 respectively). As might be expected for cyclic loading, these came close to, but remained slightly below, the lines representing the critical stress ratios of the materials in monotonic loading identified by Gräbe and Clayton (2009: Figure 7).

CONCLUSIONS

The behaviour of four saturated sand-clay mixes with particle size distributions typical of railway track foundation were investigated under cyclic loading conditions involving principal stress rotation. The following conclusions can be drawn.

1. Increasing the clay content from 7% to 14% by dry weight increased the cyclic shear stress threshold at which significant axial strain and excess pore pressures started to accumulate in undrained tests. Increasing the clay content to 24% gave no further increase in the cyclic stress threshold, although the associated axial strain did increase slightly.

2. After the cyclic shear stress threshold had been exceeded, the rate of pore pressure increase with the logarithm of the axial strain $\mathrm{d}R/\mathrm{d}(\log_{10}\varepsilon_a)$ was similar for the materials having clay contents of 7% and 24%, greater for the material having a clay content of 14%, and greatest for a clay content of 11%.

3. Increasing the clay content to 24% increased the resilient modulus for stress cycles below the cyclic shear stress threshold by up to about 20%. More significantly, increasing the clay content reduced the rate of stiffness degradation to ~0.03MPa/cycle once the cyclic shear stress threshold was exceeded, compared with a rate of ~0.10 MPa/cycle for the materials having clay contents of 11% and 14%.

4. Excess pore pressure generation reduced with increases in both the intergranular and the global void ratios and after the cyclic shear stress threshold had been exceeded, also with strain. However, the relationship between excess pore pressure and intergranular void ratio showed considerably more scatter, suggesting that the relationship with global void ratio strain is probably a more useful indicator.

ACKNOWLEDGEMENTS

The research was carried out with the financial support of the Engineering and Physical Sciences Research Council (grant number EP/H044949/1, *Railway Track for the 21st Century*).

NOTATION

B	Skempton's pore water pressure coefficient
E	Resilient Young's Modulus
e_{glob}	Global void ratio
$e_{intergr}$	Intergranular void ratio
F	Axial force
GDS	Global Digital Systems
G_s	Grain specific gravity (particle density)
$G_{s\,sand}$	Specific gravity of sand
$G_{s\,silt}$	Specific gravity of silt
$G_{s\,clay}$	Specific gravity of clay
H	Specimen height
HCA	Hollow cylinder apparatus
HPC	Hymod prima clay
LBSFB	Leighton Buzzard sand fraction B
LBSFC	Leighton Buzzard sand fraction C
LBSFD	Leighton Buzzard sand fraction D
LVDT	Linear variable differential transformer
M	Stress ratio q/p' at the critical state
M_{sand}	Mass of sand
M_{silt}	Mass of silt
M_{clay}	Mass of clay
N	Number of cycles
OCR	Overconsolidation ratio
p'	Mean effective stress = $\left(\frac{\sigma'_1+\sigma'_2+\sigma'_3}{3}\right)$

PSR	Principal stress rotation
q	Deviator stress = $\frac{1}{\sqrt{2}}\sqrt{(\sigma'_1-\sigma'_2)^2+(\sigma'_1-\sigma'_3)^2+(\sigma'_2-\sigma'_3)^2}$
r_i	Inner radius
T	Torque
u	Excess pore water pressure
V_i	Initial inner specimen volume
Δ	Prefix denoting incremental change
ε_a	Axial strain
σ_z	Axial stress
$\tau_{\theta z}$	Shear stress
ρ_{water}	Density of water

REFERENCES

Amini, F., Qi, G. 2000. Liquefaction testing of stratified silty sands. *Journal of Geotechnical and Geoenvironmental Engineering* **126**, No. 3, 208-217.

AREA 1996. Manual for Railway Engineering, *American Railway Engineering Association* **1**, Washington, D.C.

Black, D. K., and Lee, K. L. 1973. Saturating laboratory samples by back pressure. *Journal of the Soil Mechanics and Foundations Division* **99**, No. 1, 75-93.

Bray, J. D., and Sancio, R. B. 2006. Assessment of the liquefaction susceptibility of fine-grained soils. *Journal of Geotechnical and Geoenvironmental Engineering* **132**, No. 9, 1165–1177.

Brown, S. F., Lashine, A. K. F., and Hyde, A. F. L. 1975. Repeated load triaxial testing of a silty clay. *Géotechnique* **25**, No. 1, 95-114.

Brown, S. F. 1996. Soil mechanics in pavement engineering. *Géotechnique* **46**, No. 3, 383-426.

Cai, Y., Sun, Q., Guo, L., Juang, C.H., and Wang, J. 2015. Permanent deformation characteristics of saturated sand under cyclic loading. *Canadian Geotechnical Journal* **52**, No. 6, 795–807.

Chan, F. W. K., and Brown, S. F. 1994. Significance of principal stress rotation in pavements. *Proceedings of the 13th International Conference on Soil Mechanics and Foundation Engineering,* New Delhi, India*,* 5-10 January 1994. Taylor & Francis, New York, 1823-1826.

Clayton, C. R. I., and Khatrush, S. A. 1986. A new device for measuring local axial strains on triaxial specimens. *Géotechnique* **36**, No. 4, 593-597.

Cuccovillo, T., and Coop, M. R. 1997. The measurement of local axial strains in triaxial tests using LVDTs. *Géotechnique* **47**, No. 1, 167-171.

Erten, D., and Maher, M. H. 1995. Cyclic undrained behavior of silty sand. *Soil Dynamics and Earthquake Engineering* **14**, No. 2, 115–123.

Gräbe, P. J. 2001. *Resilient and permanent deformation of railway foundations under principal stress rotation*. Ph.D. thesis, University of Southampton.

Gräbe, P. J., and Clayton, C. R. I. 2009. Effects of principal stress rotation on permanent deformation in rail track foundations. *Journal of Geotechnical and Geoenvironmental Engineering* **135**, No. 4, 555-565.

Gräbe, P. J., and Clayton, C. R. I. 2014. Effects of principal stress rotation on resilient behavior in rail track foundations. *Journal of Geotechnical and Geoenvironmental Engineering* **140**, No. 2, 1-10.

Guo, L., Cai, Y., Jardine, R. J., Yang, Z., and Wang, J. 2017. Undrained behaviour of intact soft clay under cyclic paths that match vehicle loading conditions. *Canadian Geotechnical Journal*, Ahead of print, https://doi.org/10.1139/cgj-2016-0636

Hight, D. W., Gens, A., and Symes, M. J. 1983. The development of a new hollow cylinder apparatus for investigating the effects of principal stress rotation in soils. *Géotechnique* **33**, No. 4, 355-383.

Indraratna, B., Biabani, M., and Nimbalkar, S. 2015. Behavior of geocell-reinforced subballast subjected to cyclic loading in plane-strain condition. *Journal of Geotechnical and Geoenvironmental Engineering* **141**, No. 1, 1-16.

Jardine, R. J., Symes, M. J., and Burland, J. B. 1984. The measurement of soil stiffness in the triaxial apparatus. *Géotechnique* **34**, No. 3, 323-340.

Mamou, A., Powrie, W., Priest, J. A., and Clayton, C. R. I. 2017. The effects of drainage on the behaviour of railway track foundation materials during cyclic loading. *Géotechnique,* Ahead of print, http://dx.doi.org/10.1680/jgeot.15.P.278.

Mamou, A. 2013. *Effects of principal stress rotation and drainage on the resilient stiffness of railway foundations*. Ph.D. thesis, University of Southampton.

Mitchell, J. K. 1976. *Fundamentals of soil behavior*, Wiley, New York.

O'Reilly, M. P., Brown, S. F., and Overy, R. F. 1991. Cyclic loading of silty clay with drainage periods. *Journal of Geotechnical Engineering* **117**, No. 2, 354-362.

Otter, L., Clayton, C. R. I., Priest, J. A., and Grabe, P. J. 2015.The stiffness of unsaturated railway formations. *Proceedings of the Institution of Mechanical Engineers, Part F: Journal of Rail and Rapid Transit* **230***,* No.4, 1040-1052.

Polito, C. P., and Martin, II, J. R. 2001. Effects of nonplastic fines on the liquefaction resistance of sands. *Journal of Geotechnical and Geoenvironmental Engineering* **127**, No. 5, 408-415.

Powrie, W., Yang, L. A., and Clayton, C. R. I. 2007. Stress changes in the ground below ballasted railway track during train passage. *Proceedings of the Institution of Mechanical Engineers, Part F: Journal of Rail and Rapid Transit* **221**, No. 2, 247-261.

Priest, J. A., Powrie, W., Yang, L., Gräbe, P. J., and Clayton, C. R. I. 2010. Measurements of transient ground movements below a ballasted railway line. *Géotechnique* **60**, No. 9, 667-677.

Shahu, J. T., Yudhbir, and Rao, K. 1999. A simple test methodology for soils under transportation routes. *Géotechnique* **49**, No. 5, 639-649.

Statistical Software Inc. 1994. *Sigma Plot*. Statistical Software Inc, San Jose, CA

Tatsuoka, F., Sonoda, S., Hara, K., Fukushima, S., and Pradhan, T. B. S. 1986. Failure and deformation of sand in torsional shear. *Soils and Foundations* **26**, No. 4, 79-97.

Vucetic, M., and Dobry, R. 1988. Cyclic triaxial strain-controlled testing of liquefiable sands. ASTM Spec. Tech. Publ. **977**, ASTM, Philadelphia, Pa., 475–485.

Table 1: *Compositions of materials A to D (as a percentage of total dry specimen weight) as formulated by Gräbe and Clayton (2014).*

		Reconstituted material			
Component	**Grain size range**	**A**	**B**	**C**	**D**
		Percentages by weight of constituents			
Sand (Leighton Buzzard) G_s = 2.65	Fraction B600µm-1.180mm	51	46	43	32
	Fraction C300-600 µm	11	10	9	7
	Fraction D150-300 µm	11	10	9	7
Silt (HPF5) G_s = 2.65	5-150 µm	19	21	23	27
Clay (HPC) G_s = 2.60	< 125 µm	8	13	16	27
		Resulting composition of mixes (%)			
Sand content		79	73	68	54
Silt content		14	16	18	22
Clay content		7	11	14	24

Table 2: *Clay contents, water content, dry densities and corresponding global and intergranular void ratios of the investigated sand-clay mixes.*

Material as tested	Clay content (%)	Water content (%)	Dry density (Mg/m^3)	Global void ratio	Intergranular void ratio
A	7%	7.88	2.15	0.23	0.69
B	11%	8.31	2.12	0.25	0.87
C	14%	8.47	2.12	0.25	1.05
D	24%	8.61	2.10	0.26	1.75

Table 3: *Summary of the testing programme and key results.*

Cyclic preloading stages (free-to-drain)

Test	**Material type (clay content)**	$\Delta\tau_{\theta z}$	**Number of cycles**
FA8.5P	A (7%)	$\Delta\tau_{\theta z}$ =+8.5 → −8.5kPa	710
FA11.5P		$\Delta\tau_{\theta z}$ =+11.5 → −11.5kPa	710
FB8.5P	B (11%)	$\Delta\tau_{\theta z}$ =+8.5 → −8.5kPa	708
FB11.5P		$\Delta\tau_{\theta z}$ =+11.5 → −11.5kPa	700
FC8.5P	C (14%)	$\Delta\tau_{\theta z}$ =+8.5 → −8.5kPa	712
FC11.5P		$\Delta\tau_{\theta z}$ =+11.5 → −11.5kPa	710
FD8.5P	D (24%)	$\Delta\tau_{\theta z}$ =+8.5 → −8.5kPa	700
FD11.5P		$\Delta\tau_{\theta z}$ =+11.5 → −11.5kPa	700

Undrained stages

Test	**Test stage**	**Material type (clay content)**	$\Delta\tau_{\theta z}$	**Number of cycles**	**Resilient modulus**(measured at the end of each test stage)	**Cyclic shear stress threshold**
UA8.5	a	A (7%)	$\Delta\tau_{\theta z}$ =+8.5 → −8.5kPa	729	58MPa	≤8.5kPa
UB8.5	a	B (11%)	$\Delta\tau_{\theta z}$ =+8.5 → −8.5kPa	710[2]	87MPa	11.5kPa
UB11.5	b		$\Delta\tau_{\theta z}$ =+11.5 → −11.5kPa	321	61MPa	
UC8.5	a	C (14%)	$\Delta\tau_{\theta z}$ =+8.5 → −8.5kPa	710	101MPa	14.5kPa
UC11.5	b		$\Delta\tau_{\theta z}$ =+11.5 → −11.5kPa	710	104MPa	
UC14.5	c		$\Delta\tau_{\theta z}$ =+14.5 → −14.5kPa	345	73MPa	
UD8.5	a	D (24%)	$\Delta\tau_{\theta z}$ =+8.5 → −8.5kPa	710	99MPa	
UD11.5	b		$\Delta\tau_{\theta z}$ =+11.5 → −11.5kPa	710	100MPa	

[2]Halfway through UB8.5, owing to a fault in the control system, the axial stress $\Delta\sigma_z$ remained constant and equal to 15kPa rather than being cycled between 0 and 30kPa, while the shear stress continued to be cycled between the desired values.

UD14.5	c		$\Delta\tau_{\theta z}$ =+14.5 → −14.5kPa	276	85MPa	14.5kPa

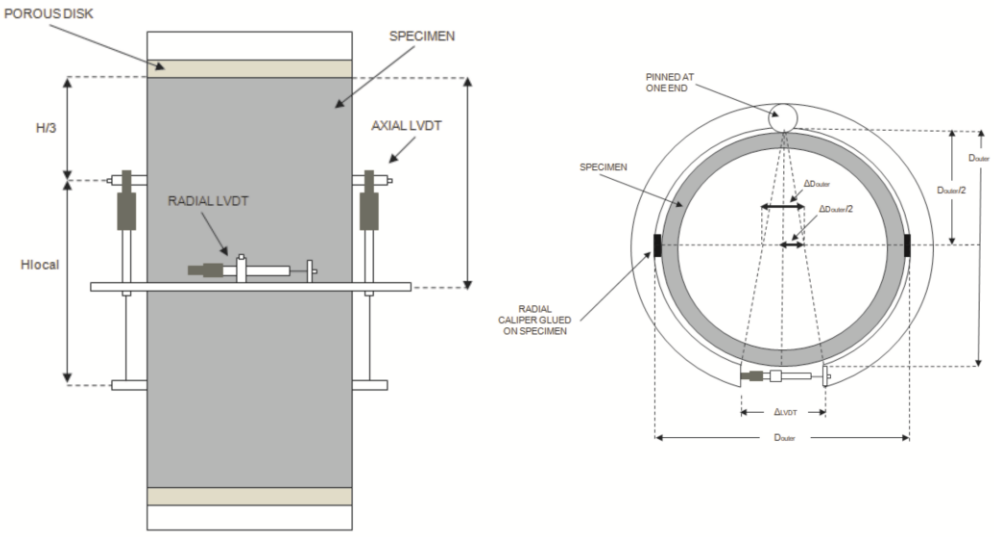

Figure 1. Schematic diagram of local instrumentation.

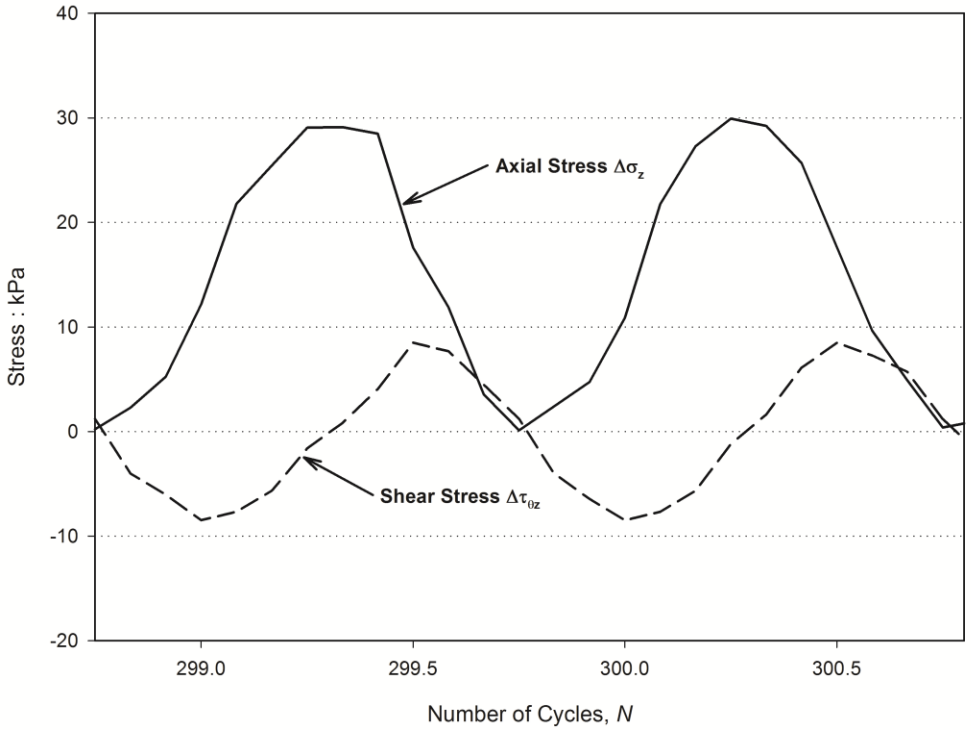

Figure 2. Typical axial and shear stress cycles, 90^0 degrees out of phase.

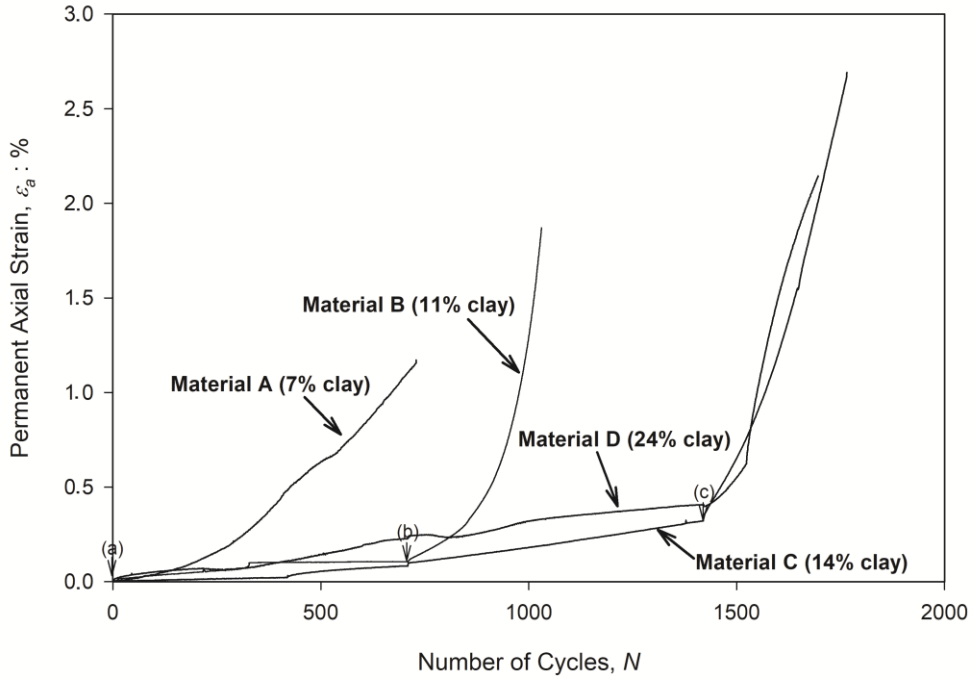

Figure 3. Permanent axial strain accumulation during undrained cyclic shear stress increases for Materials A-D (7%-24% clay).

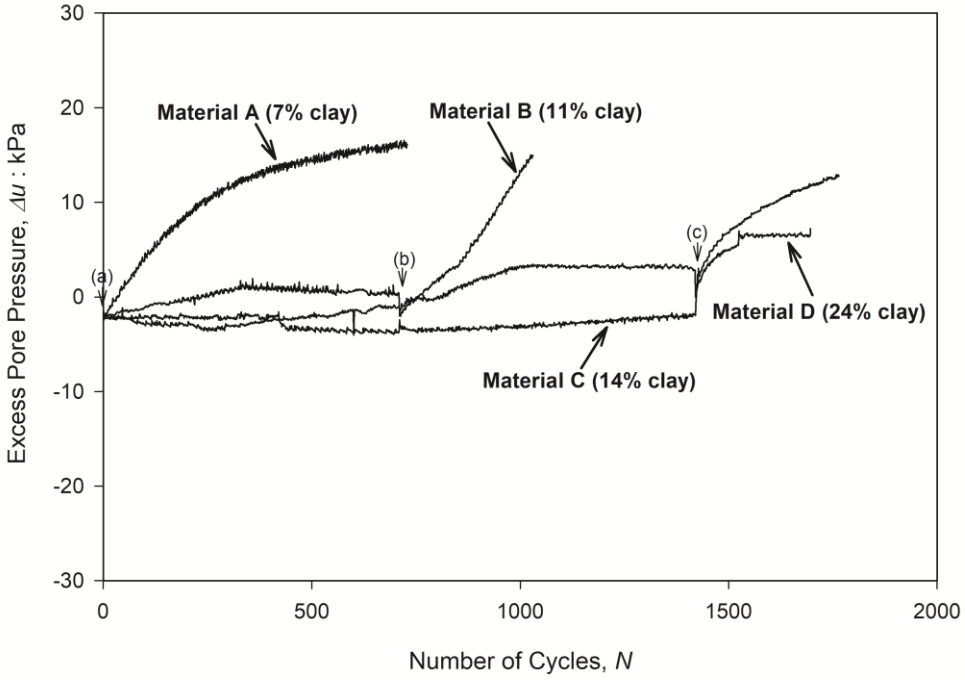

Figure 3. Permanent axial strain accumulation during undrained cyclic shear stress increases for Materials A-D (7%-24% clay).

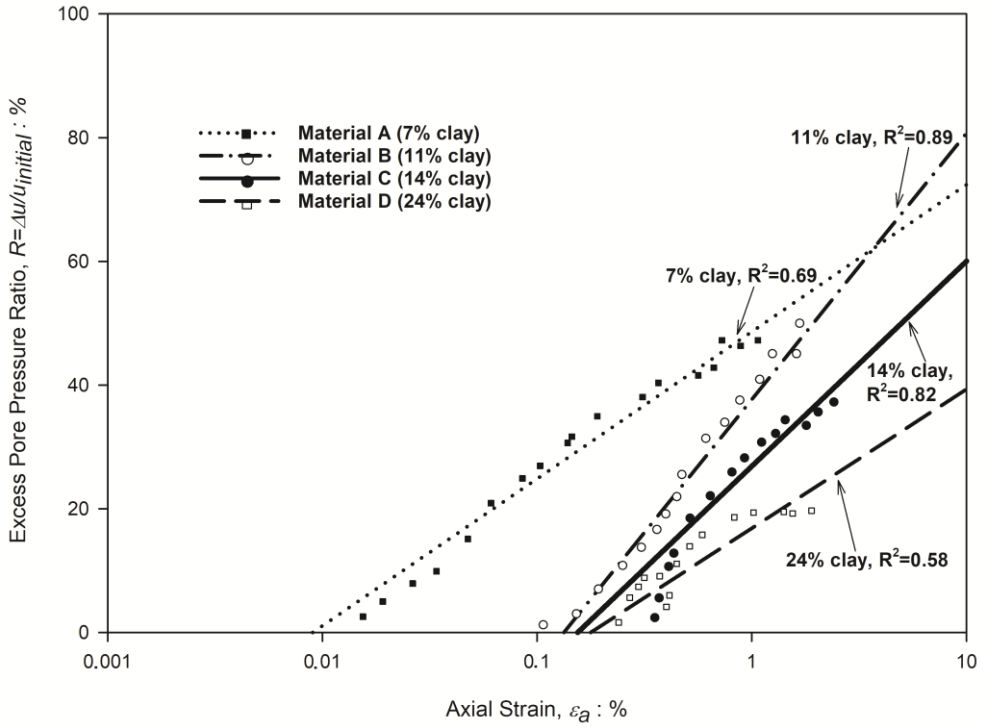

Figure 4. Residual pore pressure changes during undrained cyclic shear stress increases for Materials A-D (7%-24% clay).

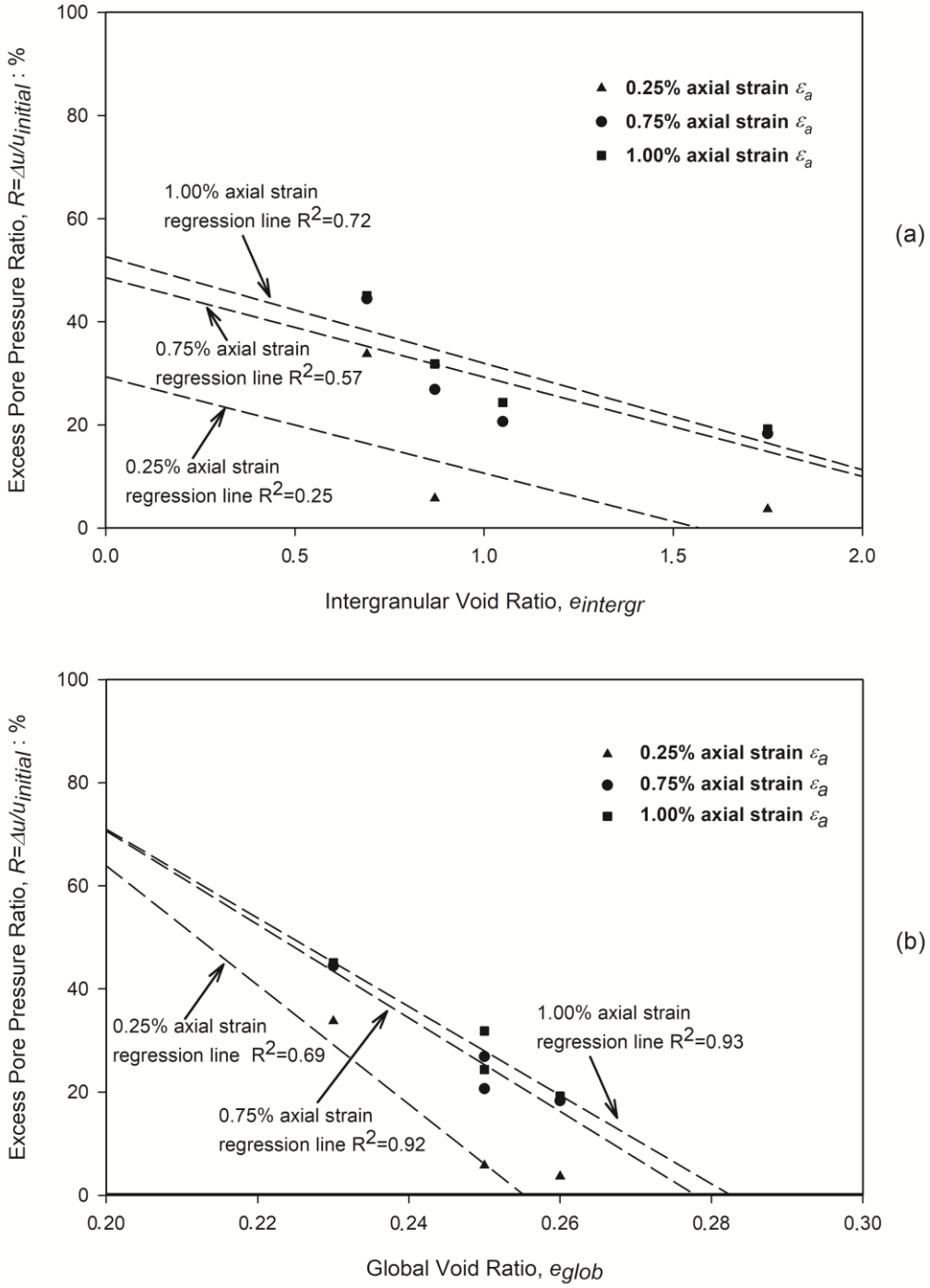

Figure 5. Excess pore pressure ratio as a function of the logarithm of axial strain for Materials A-D (7%-24% clay).

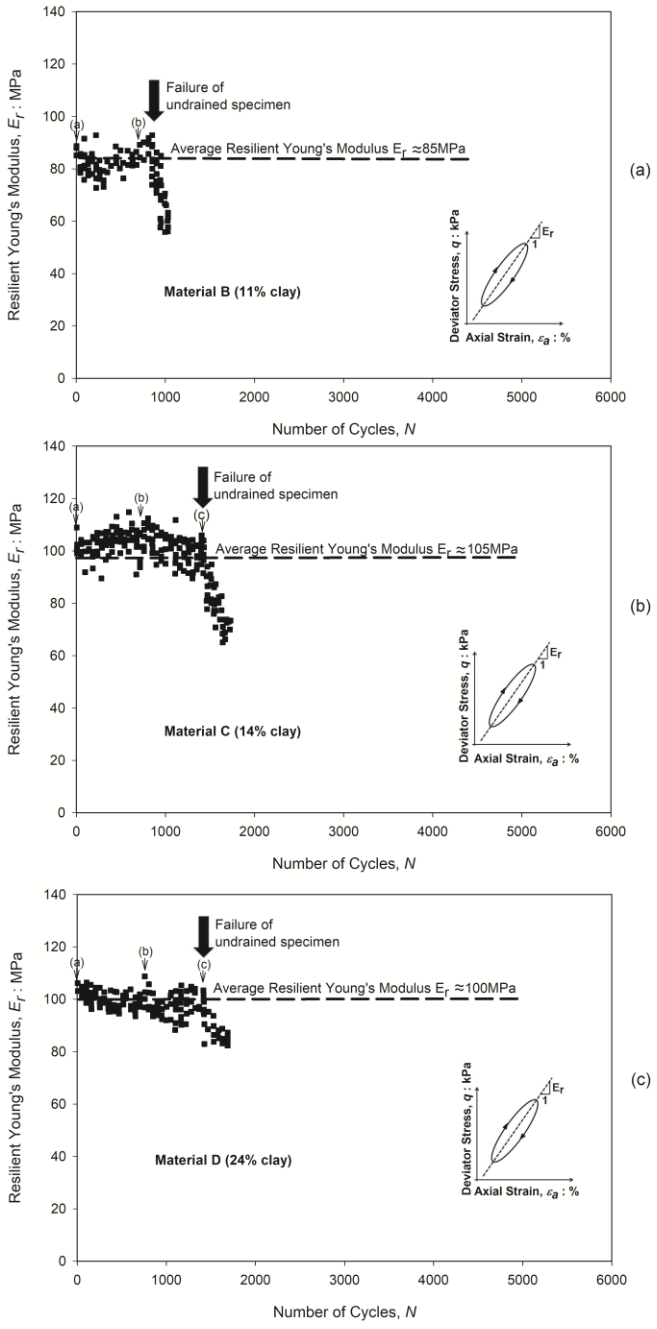

Figure 7. Changes in Resilient Young's Modulus during undrained cyclic stress increases for (a) Material B (11% clay), (b) Material C (14% clay), (c) Material D (24% clay).

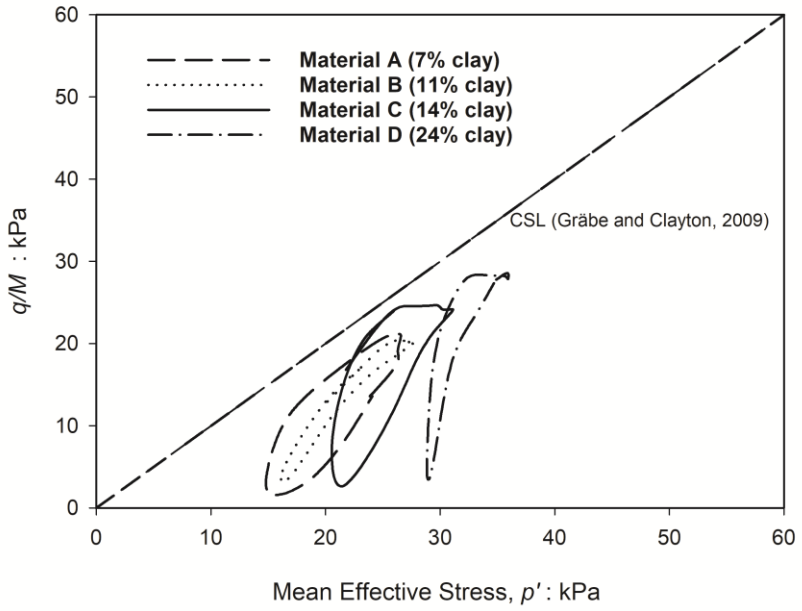

Figure 8. Stress paths (q/M vs p′) for Materials A-D (7%-24% clay): test stages causing failure (UA8.5, UB11.5, UC14.5 and UD14.5 respectively) relative to critical state lines reported by Gräbe and Clayton (2009).